Theoretical Analysis and Experimental Measurement for Resonant Vibration of Piezoceramic Circular Plates

Chi-Hung Huang, Yu-Chih Lin, and Chien-Ching Ma

***Abstract*—Based on the electroelastic theory for piezoelectric plates, the vibration characteristics of piezoceramic disks with free-boundary conditions are investigated in this work by theoretical analysis, numerical simulation, and experimental measurement. The resonance of thin piezoceramic disks is classified into three types of vibration modes: transverse, tangential, and radial extensional modes. All of these modes are investigated in detail. Two optical techniques, amplitude-fluctuation electronic speckle pattern interferometry (AF-ESPI) and laser Doppler vibrometer (LDV), are used to validate the theoretical analysis. Because the clear fringe patterns are shown only at resonant frequencies, both the resonant frequencies and the corresponding mode shapes are obtained experimentally at the same time by the proposed AF-ESPI method. Good quality of the interferometric fringe patterns for both the transverse and extensional vibration mode shapes are demonstrated. The resonant frequencies of the piezoceramic disk also are measured by the conventional impedance analysis. Both theoretical and experimental results indicate that the transverse and tangential vibration modes cannot be measured by the impedance analysis, and only the resonant frequencies of extensional vibration modes can be obtained. Numerical calculations based on the finite element method also are performed, and the results are compared with the theoretical analysis and experimental measurements. It is shown that the finite element method (FEM) calculations and the experimental results agree fairly well for the resonant frequencies and mode shapes. The resonant frequencies and mode shapes predicted by theoretical analysis and calculated by finite element method are in good agreement, and the difference of resonant frequencies for both results with the thickness-to-diameter (h/D) ratios, ranging from 0.01 to 0.1, are presented.**

I. Introduction

Since Pierre and Jacques Curie discovered the piezoelectric effect in 1880, there has been much further research and applications [1], [2]. Currently, piezoelectric materials are widely used in electromechanical sensors, actuators, nondestructive testing devices, and electro-optic modulators. The piezoelectric effect is applied to many modern engineering applications because it expresses the connection between the electrical and mechanical fields. Although the vibration characteristics of piezoelectric materials can be determined by the linear piezoelasticity, the Maxwell equation and piezoelectric constitutive equations [3], it is difficult to obtain analytical solutions for even a simple geometry. In general, there are two numerical methods that are usually used to study the vibration problem of piezoelectric materials: one is the variational approximation method and the other is finite element analysis. Eer Nisse [4] applied the calculus of variation to the analysis of piezoelectric disks and compared the results to the experimental results obtained by Shaw [5]. Holland [6] used the Rayleigh-Ritz method to study the extensional modes of rectangular piezoelectric plates and classified them into four distinct symmetry types. Kunkel *et al.* [7] studied the vibration modes of PZT-5H ceramics disks concerning the thickness-to-diameter (h/D) ratio ranging from 0.1 to 5. Due to the great flexibility and extensive applicability, the finite element method has become the alternative method to the analysis of piezoelectric material in various configurations. Ivina [8] studied the symmetric modes of vibration for circular piezoelectric plates to determine the resonant and antiresonant frequencies, radial mode configurations, and optimum geometrical dimensions to maximize the dynamic electromechanical coupling coefficient. Guo *et al.* [9] presented the results for PZT-5A piezoelectric disks with h/D of 0.05 and 0.1. In that study there were five types of modes classified according to the mode shape characteristics, and the physical interpretation was clarified. The finite element method is a powerful tool, but sometimes an analytical solution is needed to get a deep and clear understanding of the characteristics of resonant vibrations for piezoceramic plates.

In addition to variational and finite element methods, optical techniques usually are used for experimental measurement of resonant frequencies of piezoelectric plates. Shaw [5] used an optical interference technique in which a stroboscopically illuminated multiple beam was applied to measure the surface motion of thick barium titanate disks. However, only normal modes having symmetry with respect to the axis and to the central plane were observed. Minoni and Docchio [10] proposed an optical self-calibrating technique, based on the signal-processing chain, to measure the vibration amplitude of PZTs for different operating frequencies. To evaluate the piezoelectric constants, Ohki *et al.* [11] used the fiber-optic technique to measure the vibration amplitude of piezoceramic circular rod and disk. Chang [12] used the dual-beam

Manuscript received March 10, 2003; accepted July 23, 2003.

C.-H. Huang is with the Department of Mechanical Engineering, Ching Yun University, Chung-Li, Taiwan 320, Republic of China.

Y.-C. Lin and C.-C. Ma are with the Department of Mechanical Engineering, National Taiwan University, Taipei, Taiwan 106, Republic of China (e-mail: ccma@ntu.edu.tw).

speckle interferometry to measure the in-plane vibration amplitude on the PZT surface. As the measured displacement spectrum reaches the local maximum under some driven voltages, the resonant frequencies of in-plane modes were determined. To obtain the vibration mode shapes simultaneously, the technique with full-field measurement capability should be used. Koyuncu [13] used electronic speckle pattern interferometry (ESPI) with reference beam modulation to study the vibration amplitudes and vibration modes of PZT-4 transducers in air and water. Oswin *et al.* [14] used ESPI to validate the finite element model of flextensional transducer with an elliptical shape, studying both in-plane and out-of-plane vibrations. Ma and Huang [15], [16] used the amplitude-fluctuation (AF)-ESPI method to investigate the three-dimensional vibration of piezoelectric rectangular parallelepipeds and cylinders, and presented both the resonant frequencies and mode shapes.

Because piezoceramic transducers are usually circular, the vibration characteristics of piezoceramic disks are important in transducer design and application. Though algorithms based on the finite element method are able to solve this problem, theoretical methods often are preferred because the numerical approaches do not give sufficient insight into the physical interpretation of the resonant vibration of piezoceramic plates. If the piezoceramic disk is thin, the out-of-plane (transverse) vibration and the in-plane (tangential and extensional) vibration are uncoupled. In this study, we will analyze in detail the vibration behavior for transverse, tangential, and extensional vibrations, including the resonant frequencies, mode shapes, and electrical currents. The nonaxisymmetric modes are investigated for the transverse vibration, and tangential and extensional vibrations are restricted to axisymmetric modes. To validate the theoretical results, two optical techniques—namely, AF-ESPI and laser Doppler vibrometer (LDV)—and the electrical impedance measurement are used to experimentally investigate the vibration behavior of piezoceramic disks in resonance. The advantage of using the AF-ESPI method is that not only resonant frequencies but also the corresponding mode shapes for transverse and extensional modes can be obtained. The fringe patterns of AF-ESPI shown in the experimental results correspond to the vibrating mode shapes. According to experimental results obtained in this study, it is shown that only the radial extensional vibration for the piezoceramic disk can be measured by the impedance analysis, and it also is verified by theoretical analysis. In addition to the AF-ESPI measurement, the resonant frequencies of transverse vibration modes also are determined by a LDV system. A commercially available finite element software program is used to provide the numerical calculations. Good agreements of the mode shapes and resonant frequencies are obtained for experimental and theoretical results. And, numerical FEM calculations are performed, and the accuracy of theoretical results are presented in this study for different thickness-to-diameter (h/D) ratios are verified by the results of finite element analyses.

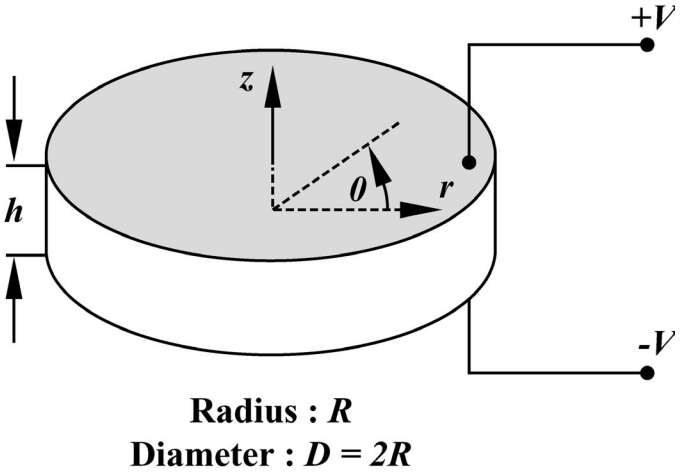

Fig. 1. Geometry and coordinate system of the piezoceramic disk.

II. Theoretical Analysis of Dynamic Characteristics for Circular Piezoceramic Disks

Fig. 1 shows the geometrical configuration of a piezoceramic disk with radius R and thickness h; the cylindrical coordinates (r, θ, z) with the origin in the center of the disk are used. The piezoceramic disk is polarized in the thickness direction, and the two opposite faces of the disk are covered with complete electrodes. The system of governing equations and basic hypotheses needed to analyze the vibration characteristics of the piezoceramic disk is presented following Rogacheva [17]. The differential equations of equilibrium in cylindrical coordinates are:

$$\frac{\partial \sigma_{rr}}{\partial r} + \frac{1}{r}\frac{\partial \sigma_{r\theta}}{\partial \theta} + \frac{\partial \sigma_{rz}}{\partial z} + \frac{1}{r}(\sigma_{rr} - \sigma_{\theta\theta}) + \rho\frac{\partial^2 u}{\partial t^2} = 0, \tag{1a}$$

$$\frac{\partial \sigma_{r\theta}}{\partial r} + \frac{1}{r}\frac{\partial \sigma_{\theta\theta}}{\partial \theta} + \frac{\partial \sigma_{\theta z}}{\partial z} + \frac{2}{r}\sigma_{r\theta} + \rho\frac{\partial^2 v}{\partial t^2} = 0, \tag{1b}$$

$$\frac{\partial \sigma_{rz}}{\partial r} + \frac{1}{r}\frac{\partial \sigma_{\theta z}}{\partial \theta} + \frac{\partial \sigma_{zz}}{\partial z} + \frac{1}{r}\sigma_{rz} + \rho\frac{\partial^2 w}{\partial t^2} = 0, \tag{1c}$$

where σ_{rr}, $\sigma_{r\theta}$, $\sigma_{\theta\theta}$, σ_{zz}, σ_{rz}, $\sigma_{\theta z}$ are the components of stress; u, v and w are the displacement field in the r, θ, and z direction, respectively; and ρ is the density. The strain-mechanical displacement relations are:

$$\begin{aligned} e_{rr} &= \frac{\partial u}{\partial r}, \\ e_{\theta\theta} &= \frac{u}{r} + \frac{1}{r}\frac{\partial v}{\partial \theta}, \\ e_{zz} &= \frac{\partial w}{\partial z}, \\ e_{r\theta} &= \frac{1}{r}\frac{\partial u}{\partial \theta} + \frac{\partial v}{\partial r} - \frac{v}{r}, \\ e_{rz} &= \frac{\partial u}{\partial z} + \frac{\partial w}{\partial r}, \\ e_{\theta z} &= \frac{\partial v}{\partial z} + \frac{1}{r}\frac{\partial w}{\partial \theta}, \end{aligned} \tag{2}$$

where e_{rr}, $e_{r\theta}$, K, e_{zz} are the components of strain. The linear piezoceramic constitutive equations for a piezoceramic material with crystal symmetry class C_{6mm} are:

$$\begin{bmatrix} e_{rr} \\ e_{\theta\theta} \\ e_{zz} \\ e_{\theta z} \\ e_{rz} \\ e_{r\theta} \\ D_r \\ D_\theta \\ D_z \end{bmatrix} = \begin{bmatrix} s_{11}^E & s_{12}^E & s_{13}^E & 0 & 0 & 0 & 0 & 0 & d_{31} \\ s_{12}^E & s_{11}^E & s_{13}^E & 0 & 0 & 0 & 0 & 0 & d_{31} \\ s_{13}^E & s_{13}^E & s_{33}^E & 0 & 0 & 0 & 0 & 0 & d_{33} \\ 0 & 0 & 0 & s_{44}^E & 0 & 0 & 0 & d_{15} & 0 \\ 0 & 0 & 0 & 0 & s_{44}^E & 0 & d_{15} & 0 & 0 \\ 0 & 0 & 0 & 0 & 0 & s_{66}^E & 0 & 0 & 0 \\ 0 & 0 & 0 & 0 & d_{15} & 0 & \varepsilon_{11}^T & 0 & 0 \\ 0 & 0 & 0 & d_{15} & 0 & 0 & 0 & \varepsilon_{11}^T & 0 \\ d_{31} & d_{31} & d_{33} & 0 & 0 & 0 & 0 & 0 & \varepsilon_{33}^T \end{bmatrix} \begin{bmatrix} \sigma_{rr} \\ \sigma_{\theta\theta} \\ \sigma_{zz} \\ \sigma_{\theta z} \\ \sigma_{rz} \\ \sigma_{r\theta} \\ E_r \\ E_\theta \\ E_z \end{bmatrix}, \quad (3)$$

where s_{11}^E, s_{12}^E, K, s_{66}^E are the compliance constants; d_{15}, d_{31}, d_{33} are the piezoelectric constants; ε_{11}^T and ε_{33}^T are the dielectric constants; D_r, D_θ, D_z are the electrical displacement components, and E_r, E_θ, E_z are the electrical fields. The piezoceramic material is isotropic in the plane normal to the z-axis.

The charge equation of electrostatics is given by:

$$\frac{\partial D_r}{\partial r} + \frac{1}{r}\frac{\partial D_\theta}{\partial \theta} + \frac{1}{r}D_r + \frac{\partial D_z}{\partial z} = 0. \quad (4)$$

The electric field-electric potential relations are:

$$E_r = -\frac{\partial \varphi}{\partial r},\ E_\theta = -\frac{1}{r}\frac{\partial \varphi}{\partial \theta},\ E_z = -\frac{\partial \varphi}{\partial z}, \quad (5)$$

where φ is the electrical potential. The basic hypotheses are:

- Normal stress σ_{zz} can be neglected relative to other stresses, hence $\sigma_{zz} = 0$.
- The rectilinear element normal to the middle surface before deformation remains perpendicular to the strained surface after deformation, and its elongation can be neglected, i.e., $e_{rz} = e_{\theta z} = 0$.
- Electrical potential varies with the thickness by the square law, i.e., $\varphi = \varphi_0 + z\varphi_1 + z^2\varphi_2$; where φ_0, φ_1, and φ_2 are constants.
- Electrical displacement D_z is a constant with respect to the thickness.

According to the first and second hypotheses, the electroelasticity relation of (3) can be simplified as

$$\sigma_{rr} = \frac{1}{s_{11}^E\left(1-v_p^2\right)}\left(e_{rr} + v_p e_{\theta\theta}\right) - \frac{d_{31}}{s_{11}^E\left(1-v_p\right)}E_z, \quad (6a)$$

$$\sigma_{\theta\theta} = \frac{1}{s_{11}^E\left(1-v_p^2\right)}\left(e_{\theta\theta} + v_p e_{rr}\right) - \frac{d_{31}}{s_{11}^E\left(1-v_p\right)}E_z, \quad (6b)$$

$$\sigma_{r\theta} = \frac{1}{s_{66}^E}e_{r\theta} = \frac{e_{r\theta}}{2s_{11}^E\left(1+v_p\right)}, \quad (6c)$$

$$D_z = d_{31}\left(\sigma_{rr} + \sigma_{\theta\theta}\right) + \varepsilon_{33}^T E_z, \quad (6d)$$

in which

$$e_{rr} = \frac{\partial u_r}{\partial r} + z\frac{\partial^2 w}{\partial r^2}, \quad (7a)$$

$$e_{\theta\theta} = \frac{u_r}{r} + \frac{1}{r}\frac{\partial v_\theta}{\partial \theta} + \frac{z}{r}\left[\frac{\partial w}{\partial r} + \frac{\partial}{\partial \theta}\left(\frac{1}{r}\frac{\partial w}{\partial \theta}\right)\right], \quad (7b)$$

$$e_{r\theta} = \frac{1}{r}\frac{\partial u_r}{\partial \theta} + \frac{z}{r}\frac{\partial^2 w}{\partial r \partial \theta} + \frac{\partial v_\theta}{\partial r} + z\frac{\partial}{\partial r}\left(\frac{1}{r}\frac{\partial w}{\partial \theta}\right) - \frac{v_\theta}{r} - \frac{z}{r^2}\frac{\partial w}{\partial \theta}, \quad (7c)$$

and the planar Poisson's ratio $v_p = -\frac{s_{12}^E}{s_{11}^E}$. It is noted that $u_r = u\big|_{z=0}$ and $v_\theta = v\big|_{z=0}$ represent the radial and the tangential displacements of the middle plane.

Because the piezoceramic circular disk is thin, the out-of-plane (transverse) vibration and the in-plane (tangential and extensional) vibration are decoupled. We analyze in detail the dynamic characteristics for transverse, tangential, and extensional vibrations, including the resonant frequencies, mode shapes, and electrical currents. The nonaxisymmetric modes are investigated for transverse vibration, and tangential and extensional vibrations are restricted to axisymmetric modes.

A. Transverse Vibration

Suppose that the piezoceramic disk is driven by an alternating current (AC) voltage $Ve^{i\omega t}$ and the transverse vibration is nonaxisymmetric, the displacement in the z-direction can be assumed to have the following form:

$$w(r,\theta,t) = W(r,\theta)e^{i\omega t}, \quad (8)$$

where ω is the angular frequency. If the time-dependent term $e^{i\omega t}$ is uniformly suppressed in the analysis, by substituting (8) into (7a)–(7c), then (6a)–(6c) of the stress components can be rewritten as follows:

$$\sigma_{rr} = \frac{1}{s_{11}^E\left(1-v_p^2\right)}\left[z\frac{\partial^2 W}{\partial r^2} + v_p\frac{z}{r}\left(\frac{\partial W}{\partial r} + \frac{1}{r}\frac{\partial^2 W}{\partial \theta^2}\right)\right] - \frac{d_{31}}{s_{11}^E\left(1-v_p\right)}E_z, \quad (9a)$$

$$\sigma_{\theta\theta} = \frac{1}{s_{11}^E\left(1-v_p^2\right)}\left[\frac{z}{r}\left(\frac{\partial W}{\partial r} + \frac{1}{r}\frac{\partial^2 W}{\partial \theta^2}\right) + v_p z\frac{\partial^2 W}{\partial r^2}\right] - \frac{d_{31}}{s_{11}^E\left(1-v_p\right)}E_z, \quad (9b)$$

$$\sigma_{r\theta} = \frac{1}{s_{11}^E\left(1+v_p\right)}\left[\frac{z}{r}\frac{\partial^2 W}{\partial r \partial \theta} - \frac{z}{r^2}\frac{\partial W}{\partial \theta}\right]. \quad (9c)$$

Herein it is assumed that the stresses as indicated in (9a)–(9c) are induced by the out-of-plane displacement $W(r,\theta)$ only. The electrical potential boundary condition on the electrode-covered surfaces is:

$$\varphi\big|_{z=\pm\frac{h}{2}} = \pm V. \quad (10)$$

From (10), (9a) and (9b), the electric-field is found to be:

$$E_z = -\frac{2V}{h} - \frac{d_{31}}{\varepsilon_{33}^T} \frac{z}{s_{11}^E \left(1-v_p\right)\left(1-k_p^2\right)} \cdot \left[\frac{\partial^2 W}{\partial r^2} + \frac{1}{r}\left(\frac{\partial W}{\partial r} + \frac{1}{r}\frac{\partial^2 W}{\partial \theta^2}\right)\right], \quad (11)$$

where $k_p = \sqrt{\frac{2d_{31}^2}{\varepsilon_{33}^T S_{11}^E (1-v_p)}}$ is the planar electromechanical coupling coefficient.

Applying the integral operator $\int_{-h/2}^{h/2} \mathrm{K}\, dz$ to the equilibrium equations (1a)–(1c) and using (9a)–(9c) and (11), the governing equation of the transverse vibration has the following form:

$$D'\left[\frac{\partial^4 W}{\partial r^4} + \frac{2}{r}\frac{\partial^3 W}{\partial r^3} - \frac{1}{r^2}\frac{\partial^2 W}{\partial r^2} + \frac{1}{r^3}\frac{\partial W}{\partial r} - \frac{2}{r^3}\frac{\partial^3 W}{\partial r \partial \theta^2} + \frac{2}{r^2}\frac{\partial^4 W}{\partial r^2 \partial \theta^2} + \frac{4}{r^4}\frac{\partial^2 W}{\partial \theta^2} + \frac{1}{r^4}\frac{\partial^4 W}{\partial \theta^4}\right] - \rho h \omega^2 W = D'\nabla^4 W - \rho h \omega^2 W = 0, \quad (12)$$

where ∇^4 is a biharmonic operator and the equivalent bending stiffness is defined by:

$$D' = \frac{h^3}{12} \cdot \frac{2-(1-v_p)\,k_p^2}{2 s_{11}^E \left(1-v_p^2\right)\left(1-k_p^2\right)}. \quad (13)$$

According to (12), the general solution of nonaxisymmetric transverse vibration for the piezoceramic disk is:

$$W(r,\theta) = \left[C_1^{(n)} J_n(\beta_1 r) + C_2^{(n)} I_n(\beta_1 r)\right] \cos n\theta, \quad n = 0, 1, 2, 3, \mathrm{K}, \quad (14a)$$

in which $C_1^{(n)}$ and $C_2^{(n)}$ are constants and

$$\beta_1^4 = \frac{\rho h \omega^2}{D'} = \frac{12\rho\omega^2}{h^2} \cdot \frac{2 s_{11}^E \left(1-v_p^2\right)\left(1-k_p^2\right)}{2-(1-v_p)\,k_p^2}. \quad (14b)$$

In (14a), J_n is an nth order Bessel function of the first kind and I_n is an nth order modified Bessel function of the first kind. For the circumferential-free boundary conditions at $r = R$, we have:

$$\int_{-h/2}^{h/2} z\sigma_{rr} dz = 0, \quad (15a)$$

and

$$\int_{-h/2}^{h/2} \sigma_{rz} dz + \frac{1}{r}\frac{\partial}{\partial \theta}\int_{-h/2}^{h/2} z\sigma_{r\theta} dz = 0. \quad (15b)$$

Two systems of linear equations are obtained from (15a) and (15b), giving (16) (see next page), where $\xi = \beta_1 R$. To obtain a nontrivial solution for the constants $C_1^{(n)}$ and $C_2^{(n)}$, the determinant of coefficient matrix must be equal to zero, and that will yield the characteristic equation of resonant frequencies for nonaxisymmetric transverse vibrations as shown in (17) (see next page).

It should be noted that the values n in (17) refer to the number of nodal diameters, and the sequence of roots represents the number of nodal circles. From (14b) and (17), the resonant frequencies for nonaxisymmetric transverse vibration of piezoceramic circular plates with circumferentially-free boundary conditions are:

$$f = \frac{\xi^2 h}{2\pi R^2}\sqrt{\frac{2-(1-v_p)\,k_p^2}{24\rho s_{11}^E \left(1-v_p^2\right)\left(1-k_p^2\right)}}. \quad (18)$$

Using (14a) and (16), the transverse displacement can be expressed as given in (19) (see next page).

From (6d), the electrical current I can be expressed as:

$$\begin{aligned} I &= \frac{\partial}{\partial t}\iint_S D_z ds \\ &= i\omega \int_0^{2\pi}\int_0^R \left\{\frac{d_{31}\left(1+v_p\right) z}{s_{11}^E \left(1-v_p^2\right)}\left[\frac{\partial^2 W}{\partial r^2} + \frac{1}{r}\frac{\partial W}{\partial r} + \frac{1}{r^2}\frac{\partial^2 W}{\partial \theta^2}\right] + \left[\varepsilon_{33}^T - \frac{2d_{31}^2}{s_{11}^E\left(1-v_p\right)}\right] E_z\right\} r dr d\theta \\ &= i\omega \frac{2\pi R^2 V \varepsilon_{33}^T}{h} \cdot \left(k_p^2 - 1\right). \end{aligned} \quad (20)$$

It also should be noted that the integration in (20) can be worked out and expressed in a very simple form. It is shown clearly from (20) that the electrical current I does not approach infinity, even if the transverse vibrations are excited at resonant frequencies. This implies that the resonant frequencies of transverse vibrations cannot be measured by the impedance variation method, such as an impedance analyzer.

B. Tangential Vibration

Suppose that the tangential vibration is axisymmetric, the tangential displacement has the following form:

$$v_\theta(r,t) = \Theta(r) e^{i\omega t}. \quad (21)$$

Follow a similar procedure, after suppressing the time-dependent term $e^{i\omega t}$, the stress components for the tangential vibration can be expressed as:

$$\sigma_{rr} = \sigma_{\theta\theta} = -\frac{d_{31}}{s_{11}^E\left(1-v_p\right)} E_z, \quad (22a)$$

$$\sigma_{r\theta} = \frac{1}{2 s_{11}^E \left(1+v_p\right)}\left[\frac{d\Theta}{dr} - \frac{\Theta}{r}\right], \quad (22b)$$

where

$$E_z = -\frac{2V}{h}. \quad (22c)$$

$$C_1^{(n)}\left\{\frac{1-v_p}{1+v_p}\left[n^2J_n(\xi)-\xi J_n'(\xi)\right]-\left[\frac{1}{1+v_p}+\frac{k_p^2}{2\left(1-k_p^2\right)}\right]\xi^2J_n(\xi)\right\}$$
$$+C_2^{(n)}\left\{\frac{1-v_p}{1+v_p}\left[n^2I_n(\xi)-\xi I_n'(\xi)\right]+\left[\frac{1}{1+v_p}+\frac{k_p^2}{2\left(1-k_p^2\right)}\right]\xi^2I_n(\xi)\right\}=0, \quad (16a)$$

$$C_1^{(n)}\left\{\frac{(1-v_p)\,n^2}{1+v_p}\left[J_n(\xi)-\xi J_n'(\xi)\right]-\left[\frac{1}{1+v_p}+\frac{k_p^2}{2\left(1-k_p^2\right)}\right]\xi^3J_n'(\xi)\right\}$$
$$+C_2^{(n)}\left\{\frac{(1-v_p)\,n^2}{1+v_p}\left[I_n(\xi)-\xi I_n'(\xi)\right]+\left[\frac{1}{1+v_p}+\frac{k_p^2}{2\left(1-k_p^2\right)}\right]\xi^3I_n'(\xi)\right\}=0 \quad (16b)$$

$$\frac{\dfrac{1-v_p}{1+v_p}\left[n^2J_n(\xi)-\xi J_n'(\xi)\right]-\left[\dfrac{1}{1+v_p}+\dfrac{k_p^2}{2\left(1-k_p^2\right)}\right]\xi^2J_n(\xi)}{\dfrac{1-v_p}{1+v_p}\left[n^2I_n(\xi)-\xi I_n'(\xi)\right]+\left[\dfrac{1}{1+v_p}+\dfrac{k_p^2}{2\left(1-k_p^2\right)}\right]\xi^2I_n(\xi)}$$
$$=\frac{\dfrac{(1-v_p)\,n^2}{1+v_p}\left[J_n(\xi)-\xi J_n'(\xi)\right]-\left[\dfrac{1}{1+v_p}+\dfrac{k_p^2}{2\left(1-k_p^2\right)}\right]\xi^3J_n'(\xi)}{\dfrac{(1-v_p)\,n^2}{1+v_p}\left[I_n(\xi)-\xi I_n'(\xi)\right]+\left[\dfrac{1}{1+v_p}+\dfrac{k_p^2}{2\left(1-k_p^2\right)}\right]\xi^3I_n'(\xi)}. \quad (17)$$

$$W(r,\theta)=C_1^{(n)}\left\{J_n(\beta_1 r)-\frac{\dfrac{1-v_p}{1+v_p}\left[n^2J_n(\xi)-\xi J_n'(\xi)\right]-\left[\dfrac{1}{1+v_p}+\dfrac{k_p^2}{2\left(1-k_p^2\right)}\right]\xi^2J_n(\xi)}{\dfrac{1-v_p}{1+v_p}\left[n^2I_n(\xi)-\xi I_n'(\xi)\right]+\left[\dfrac{1}{1+v_p}+\dfrac{k_p^2}{2\left(1-k_p^2\right)}\right]\xi^2I_n(\xi)}\cdot I_n(\beta_1 r)\right\}\cos n\theta \quad (19)$$

Substituting (22) into the equilibrium (1b) and integrating over the thickness of plates, the governing equation of the tangential vibration has the following expression:

$$\frac{d^2\Theta}{dr^2}+\frac{1}{r}\frac{d\Theta}{dr}-\frac{1}{r^2}\Theta-2\rho\omega^2 s_{11}^E\left(1+v_p\right)\Theta=0. \quad (23)$$

The general solution of tangential vibrations for the piezoceramic disk is a first-kind Bessel function:

$$\Theta(r)=C_3J_1(\beta_2 r), \quad (24a)$$

in which C_3 is a constant and

$$\beta_2^2=2\rho s_{11}^E\left(1+v_p\right)\omega^2. \quad (24b)$$

With the aid of the boundary condition at $r=R$,

$$\int_{-h/2}^{h/2}\sigma_{r\theta}dz=0, \quad (25)$$

we can obtain the characteristic equation of resonant frequencies for tangential vibrations as:

$$\zeta J_0(\zeta)-2J_1(\zeta)=0,\ \zeta=\beta_2 R. \quad (26)$$

It can be shown that, by solving (26) for ζ, the tangential resonant frequencies for piezoceramic disks are:

$$f=\frac{\zeta}{2\pi R}\sqrt{\frac{1}{2\rho s_{11}^E\left(1+v_p\right)}}. \quad (27)$$

The electrical current I for tangential vibrations can be worked out as:

$$\begin{aligned} I&=\frac{\partial}{\partial t}\iint_S D_z ds\\ &=i\omega\int_0^{2\pi}\int_0^R\left\{\left[-\frac{2d_{31}^2}{s_{11}^E\left(1-v_p\right)}+\varepsilon_{33}^T\right]E_z\right\}rdrd\theta\\ &=i\omega\frac{2\pi R^2V\varepsilon_{33}^T}{h}\cdot\left(k_p^2-1\right). \end{aligned} \quad (28)$$

Hence, the resonant frequencies of tangential vibrations also cannot be measured by the impedance variation method.

C. Extensional Vibration

Suppose that the extensional vibration is axisymmetric, the radial extensional displacement of the middle plane can be assumed to be:

$$u_r(r,t) = U(r)e^{i\omega t}. \tag{29}$$

The stress-displacement relations for the extensional vibration are given by:

$$\sigma_{rr} = \frac{1}{s_{11}^E\left(1-v_p^2\right)}\left[\frac{dU}{dr}+v_p\frac{U}{r}\right]+\frac{d_{31}}{s_{11}^E\left(1-v_p\right)}\cdot\frac{2V}{h}, \tag{30a}$$

$$\sigma_{\theta\theta} = \frac{1}{s_{11}^E\left(1-v_p^2\right)}\left[\frac{U}{r}+v_p\frac{dU}{dr}\right]+\frac{d_{31}}{s_{11}^E\left(1-v_p\right)}\cdot\frac{2V}{h}, \tag{30b}$$

in which (22c) has been used. Substituting (30) into the equilibrium (1a) and integrating over the thickness of plates, we have the well-known governing equation of extensional vibrations:

$$\frac{d^2U}{dr^2}+\frac{1}{r}\frac{dU}{dr}-\frac{1}{r^2}U-\rho\omega^2 s_{11}^E\left(1-v_p^2\right)U=0. \tag{31}$$

The general solution of (31) is:

$$U(r) = C_4 J_1(\beta_3 r), \tag{32a}$$

where C_4 is a constant and

$$\beta_3^2 = \rho s_{11}^E\left(1-v_p^2\right)\omega^2. \tag{32b}$$

For the boundary condition at $r=R$, we have:

$$\int_{-h/2}^{h/2}\sigma_{rr}dz = 0. \tag{33}$$

The constant C_4 is found to be:

$$C_4 = \frac{2Vd_{31}\left(1+v_p\right)}{\left(1-v_p\right)J_1(\beta_3 R)-\beta_3 R J_0(\beta_3 R)}\frac{R}{h}. \tag{34}$$

The electrical current I for extensional vibrations can be developed as:

$$\begin{aligned} I &= \frac{\partial}{\partial t}\iint_S D_z ds = i\omega\int_0^{2\pi}\int_0^R\left\{\frac{d_{31}\left(1+v_p\right)}{s_{11}^E\left(1-v_p^2\right)}\left[\frac{dU}{dr}+\frac{U}{r}\right]\right. \\ &\quad \left.+\frac{2\varepsilon_{33}^T V}{h}\left(k_p^2-1\right)\right\}rdrd\theta \\ &= i\omega\frac{2\pi R^2 V\varepsilon_{33}^T}{h} \\ &\quad\cdot\frac{\left[1-v_p+\left(1+v_p\right)\frac{k_p^2}{k_p^2-1}\right]J_1(\beta_3 R)-\beta_3 R J_0(\beta_3 R)}{\left(1-v_p\right)J_1(\beta_3 R)-\beta_3 R J_0(\beta_3 R)}. \end{aligned} \tag{35}$$

From (35), the resonant frequencies can be found whenever the current I approaches infinity. The characteristic equation of resonant frequencies for extensional vibrations is given by:

$$\eta J_0(\eta) = \left(1-v_p\right)J_1(\eta),\ \eta=\beta_3 R. \tag{36a}$$

Eq. (36a) is the well-known result for two-dimensional analysis of the radial modes. The antiresonant frequencies for which the current through the piezoceramic disk vanishes are also important characteristics, and are determined from the roots of the following equation:

$$\left[1-v_p+\left(1+v_p\right)\frac{k_p^2}{k_p^2-1}\right]J_1(\eta) = \eta J_0(\eta). \tag{36b}$$

From (32b) and (36), the radial extensional resonant and antiresonant frequencies for piezoceramic disks with free boundary conditions can be expressed as:

$$f = \frac{\eta}{2\pi R}\sqrt{\frac{1}{\rho s_{11}^E\left(1-v_p^2\right)}}. \tag{37}$$

III. Theory of the Time-Averaged AF-ESPI Method

For the out-of-plane vibration measurement, the first image is recorded as a reference after the specimen vibrates periodically. As the vibration of the specimen continues, we assume that the vibration amplitude changes from A to $A+\Delta A$ because of the electronic noise or instability of the apparatus. When the vibration amplitude variation ΔA is rather small, subtract the first image from the second by the image processing system, and the resulting image intensity can be expressed as

$$I = \frac{\sqrt{I_0 I_r}}{2}\left|(\cos\Phi)\cdot\left[\frac{2\pi\Delta A}{\lambda}(1+\cos\Psi)\right]^2\cdot J_0\left[\frac{2\pi A}{\lambda}(1+\cos\Psi)\right]\right|, \tag{38}$$

where I_0 is the object light intensity, I_r is the reference light intensity, Φ is the phase difference between object and reference light, λ is the wavelength of laser, and Ψ is the angle between object light and observation direction.

Similar to the out-of-plane vibration case, the resulting image intensity for the in-plane vibration measurement is:

$$I = \frac{I_0}{2}\left|(\cos\Phi)\cdot\left[\frac{2\pi\Delta A'}{\lambda}\left(2\sin\Psi'\right)\right]^2\cdot J_0\left[\frac{2\pi A'}{\lambda}\left(2\sin\Psi'\right)\right]\right|, \tag{39}$$

where I_0 is the object light intensity, A' is the vibration amplitude of in-plane vibration, and Ψ' is half of the angle between two illumination lights.

From (38) and (39), we can see that the fringe patterns for both the out-of-plane and in-plane vibrations obtained

TABLE I
MATERIAL PROPERTIES OF PIC-151.

PIC-151	Ceramics
s_{11}^E (10^{-12} m^2/N)	16.83
s_{33}^E	19.0
s_{12}^E	−5.656
s_{13}^E	−7.107
s_{44}^E	50.96
s_{66}^E	44.97
d_{31} (10^{-10} m/V)	−2.14
d_{33}	4.23
d_{15}	6.1
ε_{11}^T (10^{-9} F/m)	17.134
ε_{33}^T	18.665
ρ (kg/m^3)	7800

by the AF-ESPI method are dominated by a zero-order Bessel function J_0. The AF-ESPI method for transverse vibration was first proposed by Wang *et al.* [18]. Ma and Huang [15] provided a detailed discussion of the AF-ESPI method to investigate the out-of-plane and in-plane vibrations of piezoelectric rectangular parallelepipeds for a three-dimensional configuration.

IV. Theoretical and Experimental Results

A piezoceramic disk with diameter D = 30 mm and thickness h = 1 mm is selected for experimental investigations; the modal number is PIC-151 (Physik Instrumente, Lederhose, Germany). The polarization is in the thickness direction, and two opposite faces of the specimen are fully covered by silver electrodes. The piezoceramic disk is excited by the application of an AC voltage across electrodes on the two major surfaces and has completely stress-free boundary conditions. The electroelastic properties of the test specimen PIC-151 are listed in Table I.

The schematic layout of time-averaged AF-ESPI optical systems shown in Figs. 2 and 3 are used to perform the out-of-plane and in-plane experimental measurements for resonant frequencies and corresponding mode shapes, respectively. A He-Ne laser with 30 mW and the wavelength $\lambda = 632.8$ nm is used as the coherent light source. We use a charge-coupled device (CCD) camera (Pulnix TM-7CN, Pulnix America, Inc., Sunnyvale, CA) and a frame grabber (Dipix P360F, Dipix Technologies, Inc., Ottawa, Ontario, Canada) with a digital signal processor onboard to record and process the images. As shown in Fig. 2 for the out-of-plane measurement, the laser beam is divided into two parts, the object and reference beam, by a beamsplitter. The object beam travels to the specimen, then reflects to the CCD camera. The reference beam goes directly to the CCD camera via a mirror and a reference plate. For the in-plane measurement system as shown in Fig. 3, two laser beams with the same optical path and light intensity are symmetrically incident to the specimen, then reflect to the CCD camera. The CCD camera converts the intensity distribution of the interference pattern of the object into a corresponding video signal at 30 frames per second. The signal is electronically processed then converted into an

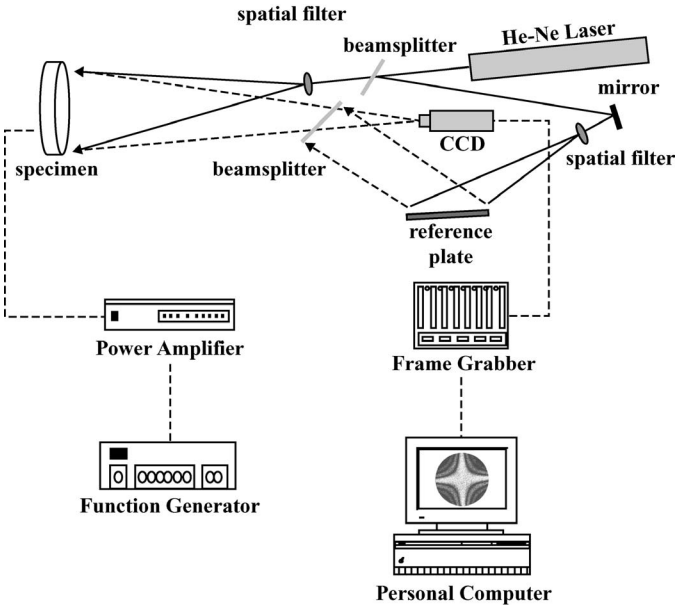

Fig. 2. Schematic of AF-ESPI setup for out-of-plane measurement.

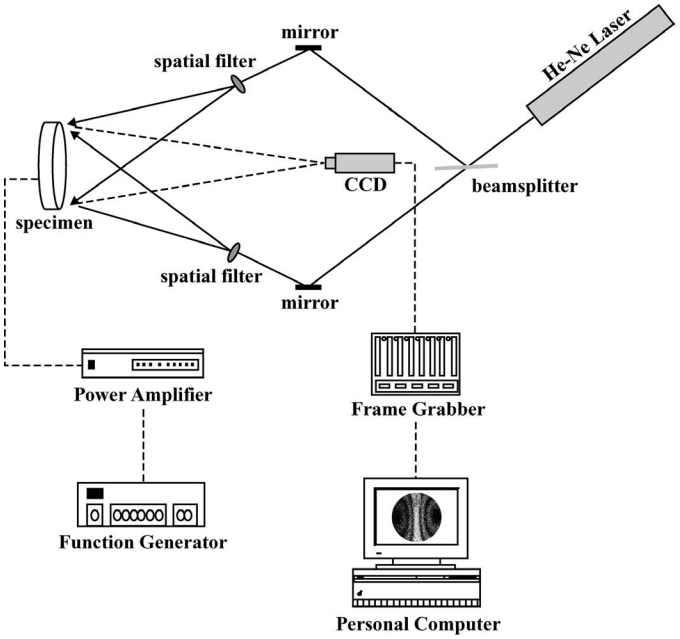

Fig. 3. Schematic of AF-ESPI setup for in-plane measurement.

image on the video monitor. Interpretation of the fringe image is similar to reading of a contour map. To achieve the sinusoidal output, a function generator (HP-33120A, Hewlett Packard, Palo Alto, CA) connected to a power amplifier (NF Electronic Instruments 4005 Type, NF Corporation, Kohokuku, Yokohama, Japan) is used.

The experimental procedure of the AF-ESPI technique is performed as follows. A reference image is taken after the piezoceramic plate is excited into vibration, then the second image is taken, and the reference image is subtracted by the image processing system. If the frequency of vibration is not the resonant frequency, only random distributed speckles are displayed, and no fringe patterns

will be shown. However, if the frequency of vibration is in the neighborhood of the resonant frequency, stationary distinct fringe patterns will be observed. Then, as the function generator is carefully and slowly adjusted, the number of fringes will increase and the fringe pattern will become more clear as the resonant frequency is approached. From the aforementioned experimental procedure, the resonant frequencies and the correspondent mode shapes can be determined at the same time.

From the AF-ESPI optical system and the experimental procedure mentioned above, the resonant frequencies and corresponding mode shapes for the transverse and extensional vibrations can be determined. In addition to the theoretical analysis and experimental measurement, finite element calculation is also performed using the commercially available software ABAQUS (Hibbit, Karlsson, and Sorensen, Inc., Pawtucket, RI) finite element package [19] in which 20-node, three-dimensional, solid piezoelectric elements (C3D20E) are selected to analyze the problem. Fig. 4 shows the experimental and numerical results for the first eight-mode shapes of transverse vibrations. Fig. 5 shows the first four-mode shapes of extensional vibrations. In Figs. 4 and 5 we indicate the phase of displacement in finite element results as solid or dashed lines, with the solid lines in the opposite direction to the dashed lines. The transition from solid lines to dashed lines corresponds to a zero displacement line, or a nodal line. The zero-order fringe, which is the brightest fringe in the experimental results, represents the nodal lines of the vibrating piezoceramic disk at resonance. The mode shapes obtained by experimental results can be checked by the nodal lines and fringe patterns with the numerical calculations. Excellent agreements of the experimental measurement and numerical calculation are found for both the transverse and extensional vibration modes.

A point-wise optical technique, LDV also was used to validate the resonant frequencies of the transverse vibration modes, and the gain spectrum of which is shown in Fig. 6. For the LDV system, a built-in dynamic signal analyzer (DSA) composed of dynamic signal analyzer software and a plug-in waveform generator board can provide the piezoceramic disk with the swept-sine excitation signal, whose gain at corresponding frequencies is analyzed by the DSA software. The peaks appearing in the frequency response curve are resonant frequencies for transverse vibrations. Table II shows the first eight transverse resonant frequencies of the piezoceramic disk obtained by using the AF-ESPI, LDV, theoretical prediction, and the FEM calculation. It is noteworthy that the theoretical predictions [i.e., from (17) and (18)] agree very well with the finite element results, with the discrepancies within 3.5%. In addition, the experimental measurements by AF-ESPI and LDV are in excellent agreement, with differences generally below 1%. The comparison of the resonant frequencies obtained from the analytical method and experimental measurements are also in good agreement.

Because the electrical impedance of piezoceramic materials drops to a local minimum when it vibrates at a resonant frequency, the resonant frequency also can be determined by an impedance analysis. Experimental impedance measurements of the piezoceramic disk are obtained by using an HP4194A impedance/gain-phase analyzer (Hewlett Packard). The impedance curve for the piezoceramic disk measured from HP4194A is shown in Fig. 7 (top) and the simulated impedance curve calculated by (35) is shown in Fig. 7 (bottom). We can see that both results are well correlated. The local minima and maxima appearing in the impedance curve correspond to resonance and antiresonance, respectively. As we expected, only the resonant frequencies of the radial extensional modes are indicated in Fig. 7 (top), i.e., those of the transverse and tangential modes cannot be obtained by the impedance analysis. This phenomenon can be explained qualitatively by means of the characteristics of piezoelectricity. When the piezoceramic plate vibrates at a resonant frequency, the charge will be strongly induced on the electrode surfaces due to the vibration deformation, called the direct piezoelectric effect, and the impedance will drop to a local minimum value. This is the reason that the resonant frequencies of piezoceramic plates can be determined by using the impedance analyzer. However, if the summation of the induced charge distributed over the electrode surfaces is zero, we are not able to find the large variation of impedance at the resonant frequency. Table III shows the first four extensional resonant frequencies of the piezoceramic disk obtained by using the AF-ESPI, impedance analysis, theoretical prediction, and FEM calculation. The discrepancy of resonant frequencies between AF-ESPI and impedance analysis is smaller than 0.3%. The theoretical predictions [i.e., from (36a) and (37)] are in excellent agreement with the finite element results and the discrepancies are within 1%, which is better than that of transverse vibration modes. The difference between the experimental measurements and analytical results may result from the determination of the material properties or the defects of the piezoceramic disk.

In view of the experimental techniques mentioned previously, we find that the tangential vibration modes cannot be obtained experimentally. Hence, only the theoretical predictions and finite element calculations are performed. Table IV shows the comparison between the theoretical predictions [i.e., from (26) and (27)] and FEM calculations for the first three tangential resonant frequencies of the piezoceramic disk. The discrepancies of both results are within 0.01%.

The electromechanical coupling coefficient is an important characteristic of piezoceramic elements used to measure the energy conversion efficiency. The dynamic electromechanical coupling coefficient proposed by Mason [20] can be computed by the expression:

$$k_d = \frac{\sqrt{f_a^2 - f_r^2}}{f_a}, \tag{40}$$

where f_r is the resonant frequency and f_a is the antiresonant frequency. This coefficient is of special interest in designing piezoelectric elements. Eq. (40) usually is used

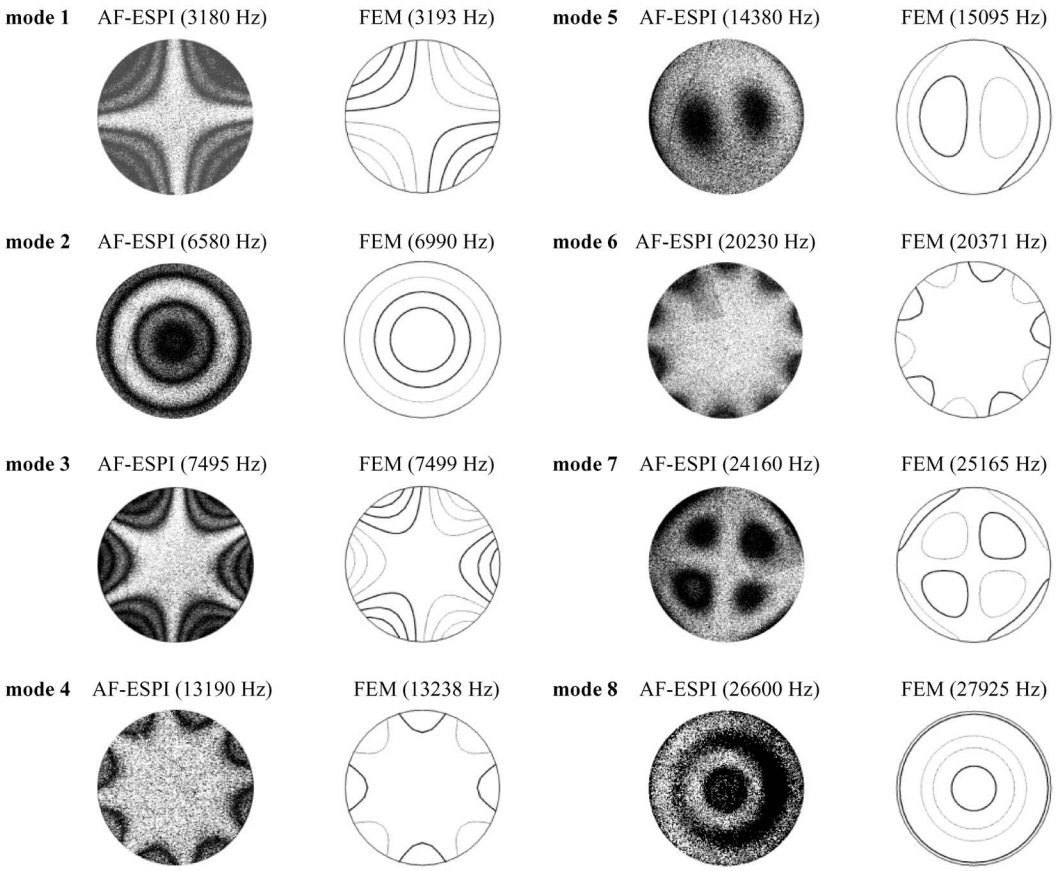

Fig. 4. Mode shapes of the transverse vibration obtained by AF-ESPI and FEM for the piezoceramic disk.

TABLE II
RESULTS OF RESONANT FREQUENCIES OBTAINED BY THEORY, FEM, LDV, AND AF-ESPI FOR THE TRANSVERSE VIBRATION.

Transverse mode	(a) Theory (Hz)	(b) FEM (Hz)	(c) LDV (Hz)	(d) AF-ESPI (Hz)	Error (a)(b)	Difference (c)(d)
1	3224	3193	3210	3180	0.97%	0.94%
2	7040	6990	6610	6580	0.72%	0.46%
3	7638	7499	7610	7495	1.85%	1.53%
4	13602	13238	13310	13190	2.75%	0.91%
5	15358	15095	14410	14380	1.74%	0.21%
6	21094	20371	20410	20230	3.55%	0.89%
7	25924	25165	24310	24160	3.02%	0.62%
8	28786	27925	26610	26600	3.08%	0.04%

TABLE III
RESULTS OF RESONANT FREQUENCIES OBTAINED BY THEORY, FEM, IMPEDANCE ANALYSIS, AND AF-ESPI FOR THE EXTENSIONAL VIBRATION.

Extensional mode	(a) Theory (Hz)	(b) FEM (Hz)	(c) Impedance (Hz)	(d) AF-ESPI (Hz)	Error (a)(b)	Difference (c)(d)
1	64397	64368	69860	69745	0.05%	0.16%
2	167789	167404	179130	179250	0.23%	−0.07%
3	266661	265147	283335	283740	0.57%	−0.14%
4	364878	360988	385558	386735	1.08%	−0.30%

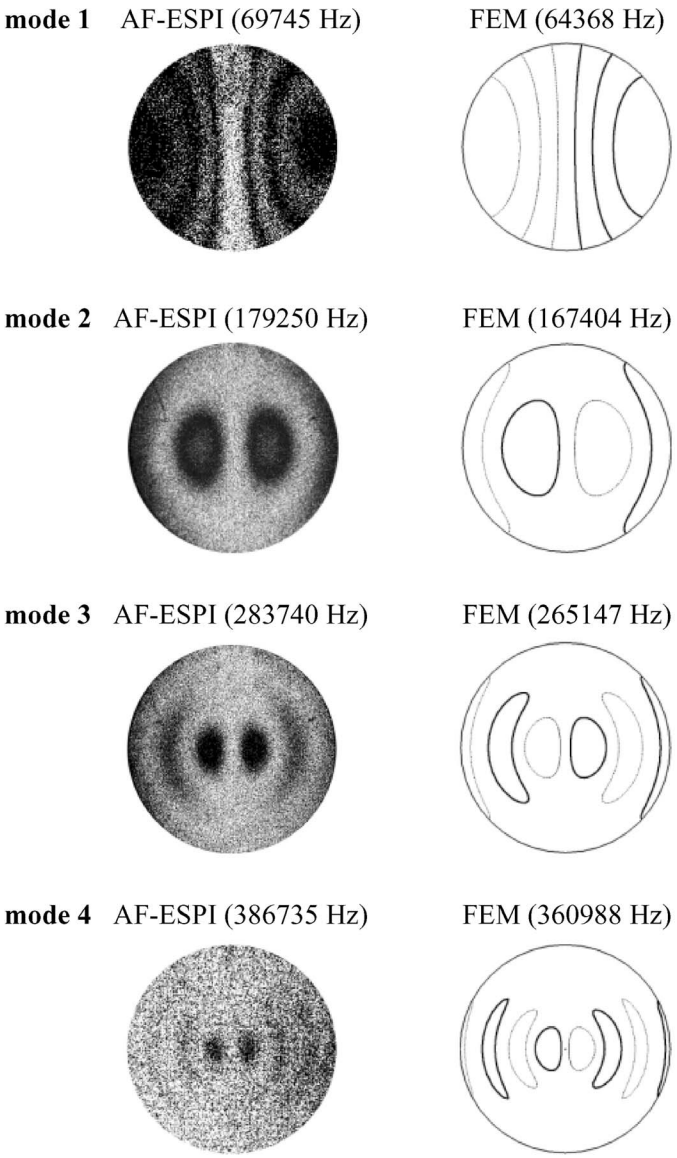

Fig. 5. Mode shapes of the extensional vibration obtained by AF-ESPI and FEM for the piezoceramic disk.

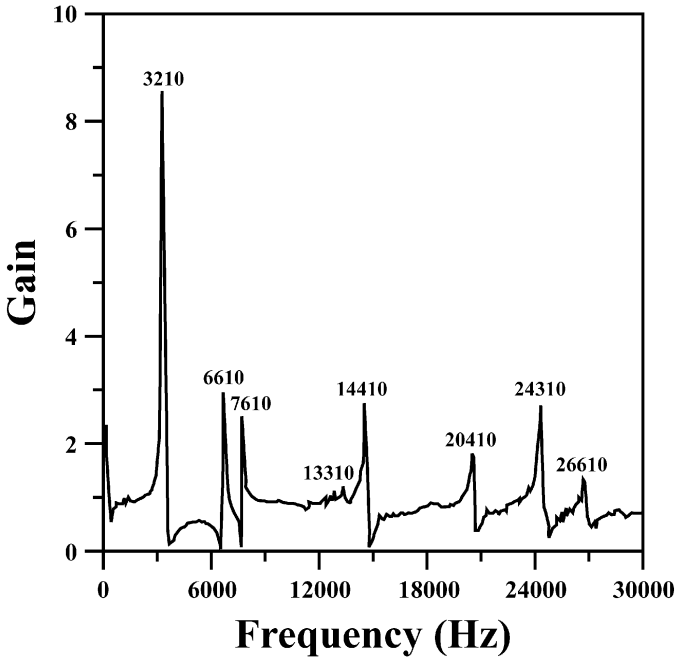

Fig. 6. LDV output gain spectrum of transverse vibrations for the piezoceramic disk.

TABLE IV
RESULTS OF RESONANT FREQUENCIES OBTAINED BY THEORY AND FEM FOR THE TANGENTIAL VIBRATION.

Tangential Mode	Theory (Hz)	FEM (Hz)	Error
1	92002	92007	−0.005%
2	150791	150801	−0.007%
3	208163	208187	−0.01%

to determine the electromechanical coupling coefficient by measuring the resonant and antiresonant frequencies. From Figs. 7(a) and (b), we can evaluate the value of k_d individually for each mode, and the results are shown in Table V for the extensional mode.

The theoretical derivation in this study is based on the assumption that the piezoceramic plat is thin, hence the theoretical predictions of resonant frequencies are accurate only if the thickness-to-diameter ratio (h/D) is small. To understand the validity of the theoretical results on the practical applications, the discrepancy between the theoretical analysis and finite element results of the resonant frequencies for transverse and extensional vibrations are shown in Figs. 8 and 9, respectively. The calculations are performed for values of h/D ranging from 0.01 to 0.1. In general, the theoretical predictions of resonant frequencies for the extensional vibration are better than those for the transverse vibration. The discrepancies of the first five modes for transverse vibration are within 5% for h/D < 0.05 and within 2% (h/D < 0.06) for the first three modes for the extensional vibration. The theoretical prediction for the first mode of extensional vibration is excellent, with discrepancy for h/D $= 0.1$ of less than 0.5%. The displacement distribution of the mode shape based on the theoretical analysis also is evaluated to compare with that of the FEM. For simplicity, only the first two axisymmetric modes of transverse and extensional vibrations are presented in Fig. 10. It is shown that two results are highly coincident for the normalized vibration amplitude in the middle plane.

V. CONCLUSIONS

Most of the previous studies for vibration analysis of piezoelectric disks are analytical and numerical results for radial extensional modes. There are very few experimental results available for the full-field configuration of mode shapes for vibrating piezoelectric disks. In this study, a

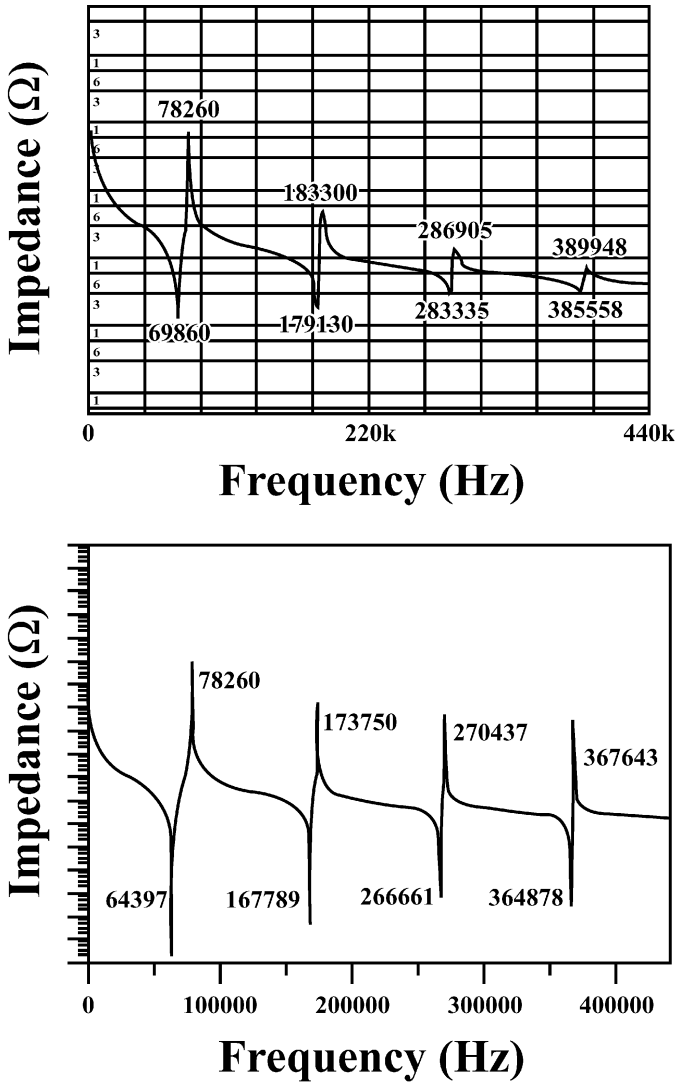

Fig. 7. Impedance variation curve of the piezoceramic disk by (top) impedance analyzer and (bottom) theoretical analysis.

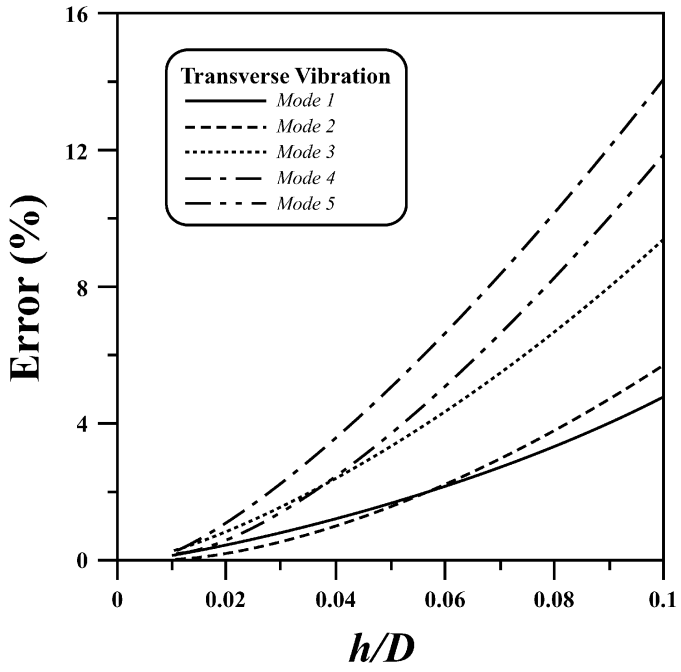

Fig. 8. Discrepancies of resonant frequency predicted by theory and numerical calculation for the transverse vibration.

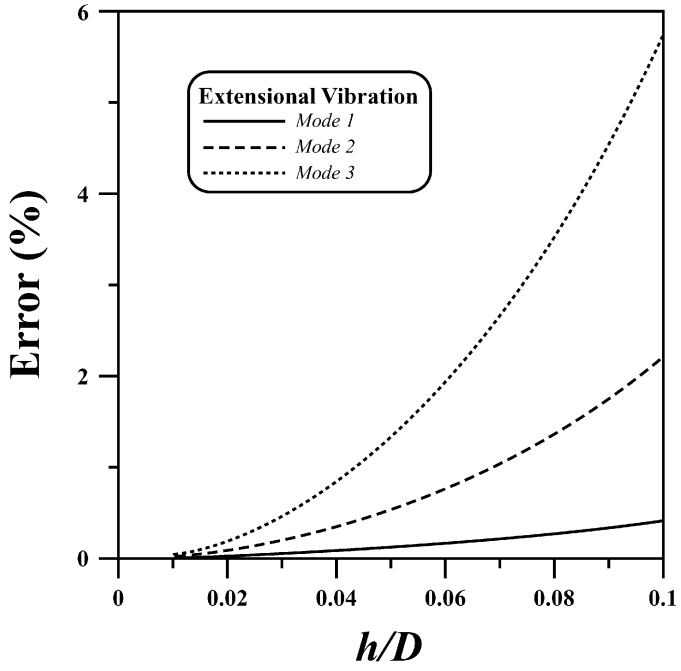

Fig. 9. Discrepancies of resonant frequency predicted by theory and numerical calculation for the extensional vibration.

TABLE V
RESULTS OF THE DYNAMIC ELECTROMECHANICAL COUPLING COEFFICIENT k_d OBTAINED BY THEORY AND FEM FOR THE EXTENSIONAL VIBRATION.

Extensional vibration	k_d (Theory)	k_d (Impedance)	Difference (%)
Mode 1	0.5832	0.4507	−22.71
Mode 2	0.2597	0.2121	−18.33
Mode 3	0.1665	0.1573	−5.56
Mode 4	0.1224	0.1479	20.86

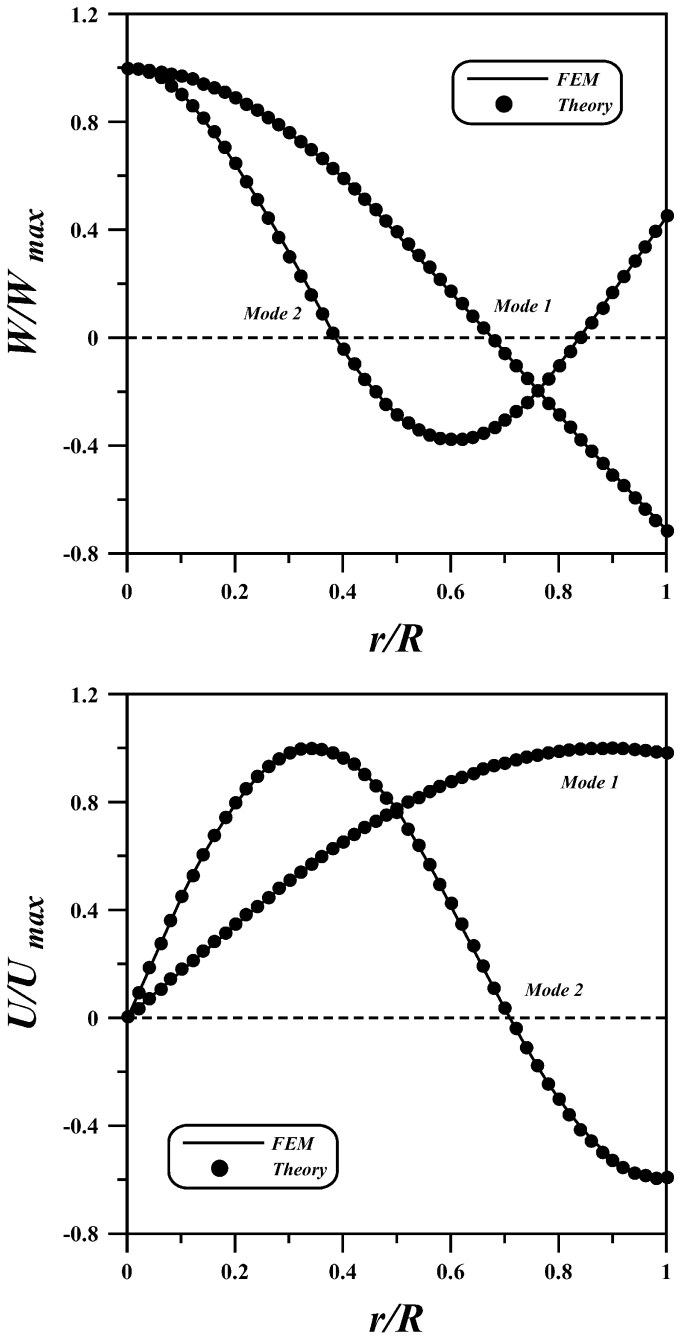

Fig. 10. Normalized displacements calculated by theory and FEM for the (top) transverse and (bottom) extensional vibrations.

self-arranged, AF-ESPI optical setup with good visibility and noise reduction has been established to simultaneously obtain both the resonant frequencies and the corresponding mode shapes of transverse and extensional vibrations.

This study investigates the vibration of piezoceramic disks with free-boundary conditions for transverse, tangential, and radial extensional modes by theoretical analysis, numerical simulation, and experimental measurement. Due to the symmetry of the material constants for piezoceramic materials, the nonaxisymmetric modes are analyzed for the transverse vibration, and tangential and extensional vibrations are restricted to axisymmetric modes. The theoretical predictions for resonant frequencies and mode shapes are presented in detail. Two optical techniques (AF-ESPI and LDV) and electrical impedance measurement are used to validate the theoretical results. Only the resonant frequencies of radial extensional vibration can be measured by the impedance analysis, and the resonant frequencies of transverse vibration are determined by the LDV system. However, both resonant frequencies and mode shapes for transverse and radial extensional vibrations are simultaneously measured by the AF-ESPI method. Good agreement of both the resonant frequencies and mode shapes are obtained for experimental measurements and theoretical predictions. The accuracy of the resonant frequencies predicted by the theoretical analysis is verified by the FEM method with the h/D ratios ranging from 0.01 to 0.1.

References

[1] D. A. Berlincourt, D. R. Curran, and H. Jaffe, "Piezoelectric and piezomagnetic materials and their function as transducers," *Phys. Acoust.*, vol. 1(A), pp. 169–270, 1964.

[2] J. Zelenka, *Piezoelectric Resonators and Their Application*. Prague, Czech Republic: Academia/Prague, 1986.

[3] H. F. Tiersten, *Linear Piezoelectric Plate Vibrations*. New York: Plenum, 1969.

[4] E. P. Eer Nisse, "Variational method for electroelastic vibration analysis," *IEEE Trans. Sonics Ultrason.*, vol. SU-14, no. 4, pp. 153–160, 1967.

[5] E. A. G. Shaw, "On the resonant vibrations of thick barium titanate disks," *J. Acoust. Soc. Amer.*, vol. 28, no. 1, pp. 38–50, 1956.

[6] R. Holland, "Contour extensional resonant properties of rectangular piezoelectric plates," *IEEE Trans. Sonics Ultrason.*, vol. SU-15, no. 2, pp. 97–105, 1968.

[7] H. A. Kunkel, S. Locke, and B. Pikeroen, "Finite-element analysis of vibrational modes in piezoelectric ceramics disks," *IEEE Trans. Ultrason., Ferroelect., Freq. Contr.*, vol. 37, no. 4, pp. 316–328, 1990.

[8] N. F. Ivina, "Numerical analysis of the normal modes of circular piezoelectric plates of finite dimensions," *Sov. Phys. Acoust.*, vol. 35, no. 4, pp. 385–388, 1990.

[9] N. Guo, P. Cawley, and D. Hitchings, "The finite element analysis of the vibration characteristics of piezoelectric discs," *J. Sound Vib.*, vol. 159, no. 1, pp. 115–138, 1992.

[10] U. Minoni and F. Docchio, "An optical self-calibrating technique for the dynamic characterization of PZT's," *IEEE Trans. Instrum. Meas.*, vol. 40, no. 5, pp. 851–854, 1991.

[11] M. Ohki, N. Shima, and T. Shiosaki, "Optical measurement of piezoelectric vibration in circular rod and disk ceramics," *Jpn. J. Appl. Phys.*, vol. 31, no. 9B, pp. 3272–3275, 1992.

[12] M. Chang, "In-plane vibration displacement measurement using fiber-optical speckle interferometry," *Preci. Eng.*, vol. 16, no. 1, pp. 36–41, 1994.

[13] B. Koyuncu, "The investigation of high frequency vibration modes of PZT-4 transducers using ESPI techniques with reference beam modulation," *Opt. Lasers Eng.*, vol. 1, pp. 37–49, 1980.

[14] J. R. Oswin, P. L. Salter, F. M. Santoyo, and J. R. Tyrer, "Electronic speckle pattern interferometric measurement of flextensional transducer vibration patterns: In air and water," *J. Sound Vib.*, vol. 172, no. 4, pp. 433–448, 1994.

[15] C. C. Ma and C. H. Huang, "The investigation of three-dimensional vibration for piezoelectric rectangular parallelepipeds by using the AF-ESPI method," *IEEE Trans. Ultrason., Ferroelect., Freq. Contr.*, vol. 48, no. 1, pp. 142–153, 2001.

[16] C. H. Huang and C. C. Ma, "Vibration characteristics for piezoelectric cylinders using amplitude-fluctuation electronic speckle

pattern interferometry," *AIAA J.*, vol. 36, no. 12, pp. 2262–2268, 1998.
[17] N. N. Rogacheva, *The Theory of Piezoelectric Shells and Plates*. Boca Raton, FL: CRC Press, 1994.
[18] W. C. Wang, C. H. Hwang, and S. Y. Lin, "Vibration measurement by the time-averaged electronic speckle pattern interferometry methods," *Appl. Opt.*, vol. 35, no. 22, pp. 4502–4509, 1996.
[19] *ABAQUS User's Manual, ver. 5.5.*. Pawtucket, RI: Hibbit, Karlsson, and Sorensen, Inc., 1995.
[20] W. P. Mason, *Piezoelectric Crystals and Their Application to Ultrasonics*. New York: Van Nostrand, 1950.

Chi-Hung Huang received his B.S., M.S., and Ph.D. degrees in mechanical engineering from the National Taiwan University, Taipei, Taiwan, Republic of China, in 1987, 1992, and 1998, respectively. Since 1998, he has worked at the Mechanical Engineering Department, Ching Yun University, Chung-Li, Taiwan, Republic of China, as an associate professor.

His current research interests include experimental optical measurement and dynamic behavior of piezoelectric materials.

Yu-Chih Lin received the B.S. degree in mechanical engineering from the National Taiwan University, Taiwan, Republic of China, and the M.S. degree in biomedical engineering from National Cheng Kung University, Taiwan, Republic of China, in 1994 and 1996, respectively. She is currently a candidate for the Ph.D. degree in the Department of Mechanical Engineering, National Taiwan University.

She currently is engaged in research on resonant characteristics of piezoelectric disks under water. Her research interests are in the fields of vibration analysis of piezoelectric materials and photomechanics.

Chien-Ching Ma received the B.S. degree in agriculture engineering from the National Taiwan University, Taiwan, Republic of China, in 1978, and the M.S. and Ph.D. degrees in mechanical engineering from Brown University, Providence, RI, in 1982 and 1984, respectively. From 1984 to 1985, he worked as a postdoc in the Engineering Division, Brown University. In 1985, he joined the faculty of the Department of Mechanical Engineering, National Taiwan University, Taiwan, Republic of China, as an associate professor. He was promoted to full professor in 1989.

His research interests are in the fields of wave propagation in solids, fracture mechanics, solid mechanics, piezoelectric material, and vibration analysis.